

# Label-Free Characterization of Amyloids and Alpha-Synuclein Polymorphs by Exploiting Their Intrinsic Fluorescence Property

Chyi Wei Chung, Amberley D. Stephens, Edward Ward, Yuqing Feng, Molly Jo Davis, Clemens F. Kaminski, and Gabriele S. Kaminski Schierle\*



Cite This: *Anal. Chem.* 2022, 94, 5367–5374



Read Online

ACCESS |



Metrics & More

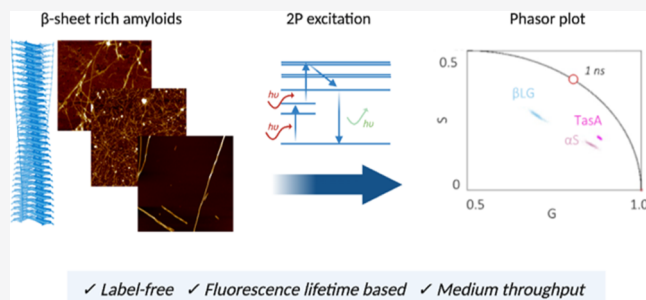


Article Recommendations



Supporting Information

**ABSTRACT:** Conventional *in vitro* aggregation assays often involve tagging with extrinsic fluorophores, which can interfere with aggregation. We propose the use of intrinsic amyloid fluorescence lifetime probed using two-photon excitation and represented by model-free phasor plots as a label-free assay to characterize the amyloid structure. Intrinsic amyloid fluorescence arises from the structured packing of  $\beta$ -sheets in amyloids and is independent of aromatic-based fluorescence. We show that different amyloids [i.e.,  $\alpha$ -Synuclein ( $\alpha$ S),  $\beta$ -Lactoglobulin ( $\beta$ LG), and TasA] and different polymorphic populations of  $\alpha$ S (induced by aggregation in salt-free and salt buffers mimicking the intra-/extracellular environments) can be differentiated by their unique fluorescence lifetimes. Moreover, we observe that disaggregation of the preformed fibrils of  $\alpha$ S and  $\beta$ LG leads to increased fluorescence lifetimes, distinct from those of their fibrillar counterparts. Our assay presents a medium-throughput method for rapid classification of amyloids and their polymorphs (the latter of which recent studies have shown lead to different disease pathologies) and for testing small-molecule inhibitory compounds.



## INTRODUCTION

Amyloid proteins aggregates share common characteristics, including a fibrillar morphology and a cross- $\beta$  sheet structure.<sup>1</sup> The majority of *in vitro* studies on the kinetics of amyloid aggregation are fluorescence based, using extrinsic fluorophores with a fluorescence intensity readout, yet this presents issues when investigating small-molecule inhibitors or fibril polymorphs (i.e., fibrils of different structures within the same amyloid species). Common extrinsic fluorophores include Congo Red (CR) and Thioflavin T (ThT) that bind by intercalating between the  $\beta$ -sheets of the amyloid of interest.<sup>2</sup> However, the binding of both CR and ThT is affected by pH and ionic concentrations,<sup>3,4</sup> which must be strictly controlled under laboratory conditions. ThT-based fluorescence assays can be affected by the binding of small inhibitory molecules or the presence of disease-associated mutants in the primary sequence affecting fibril structure; hence, the interference of fluorescence readings occurs due to either quenching effects between the molecule and ThT, or competitive binding to active sites on the amyloid protein, or the presence of different binding sites.<sup>5,6</sup> Tagging recombinant proteins with fluorescent proteins or small dye labels is also a popular method to study protein aggregation. Yet, the fluorescent protein tag can interfere with the excitation and emission of the ThT fluorescence<sup>7</sup> and large fluorescent proteins can disrupt intramolecular bonding, sterically hinder interactions, and hence alter aggregation rates.<sup>8</sup> Even the presence of small dye

molecules can influence the monomer incorporation into growing amyloid fibrils, thereby yielding polymorphic structures.<sup>9</sup>

Hence, there is motivation for the characterization of amyloid protein fibrils in a label-free manner, which can be used to investigate potential inhibitors of amyloid aggregation and structural changes to the amyloids. In our previous work, we reported the phenomenon of intrinsic amyloid fluorescence,<sup>5,10–12</sup> as corroborated by similar studies by others.<sup>13,14</sup> Characteristically, amyloid fibrils absorb light at wavelengths in the near-ultraviolet (UV) range between 340 and 380 nm, and they emit fluorescence in the visible range between 400 and 450 nm. This phenomenon is believed to be caused by electron delocalization due to the rich hydrogen-bonding networks between and within the layers of the  $\beta$ -sheets of the amyloid protein, along with the presence of short hydrogen bonds, resulting in fluorescence emission in the visible range upon UV excitation.<sup>10,11</sup> It is noted that this phenomenon is independent of the intrinsic aromatic fluorescence as observed with aromatic amino acids (e.g., tyrosine and tryptophan),

Received: December 31, 2021

Accepted: March 1, 2022

Published: March 25, 2022



which exhibit both excitation and emission in the 260–280 nm UV range rather than in the visible range as shown previously using the amyloid fibril devoid of aromatic residues,  $A\beta_{30-35}$  (AIIGLM)<sup>15</sup> and  $A\beta_{35-42}$  (MVGGVVIA).<sup>16</sup>

Here, we explore the use of intrinsic amyloid fluorescence lifetime as a potential readout for aggregation states. We choose fluorescence lifetime over fluorescence intensity, as the first is a ratiometric parameter that is independent of excitation intensity, laser scattering, and sample concentration and thickness.<sup>15</sup> Several amyloids associated with neurodegenerative diseases feature fluorescence lifetimes in the nanosecond range, with measurements that dispute whether these are mono- or complex exponential in nature.<sup>12,16</sup> Optimal excitation of amyloids is around 350–370 nm,<sup>13</sup> the wavelengths at which the power density of pulsed supercontinuum sources are very low. The alternative use of two-photon (2P) excitation, which involves the absorption of two photons at twice the wavelength but half the energy,<sup>17</sup> has inherent advantages. In contrast to single-photon excitation, which occurs through a cone of light down to the focal spot within a sample, 2P excitation (and hence any incurred photodamage) is primarily localized to the focal spot.<sup>17,18</sup> This allows for imaging without a pinhole and is more suited for dimmer samples (e.g., intrinsic amyloid fluorescence) as no photons would be rejected due to the lack of a pinhole. The low scattering property of 2P makes it suitable for deeper penetration into samples. The most common implementation involves a femtosecond titanium–sapphire (Ti:S) laser such as the one used in this work, thereby making the technique proposed more accessible for researchers as the setup is commonly available on existing 2P microscopes primarily used for deep tissue imaging.<sup>19–22</sup> Hence, we perform time-correlated single-photon counting (TCSPC) fluorescence lifetime imaging microscopy (FLIM), using 2P excitation. Moreover, we represent 2P-FLIM data on phasor plots, a global analysis approach that is efficient and parameter-free.<sup>23–25</sup> This avoids pixel-by-pixel fitting of exponential decays (i.e., a requisite of conventional exponential fitting methods), and is therefore highly efficient and less computationally expensive. Moreover, mono- and complex exponential decay lifetimes can easily be distinguished based on their positions on the phasor plot.

To determine whether 2P-FLIM can differentiate between different amyloids, we used three model amyloids, for example,  $\beta$ -lactoglobulin ( $\beta$ LG, a globular whey protein), TasA (a functional bacterial amyloid from *Bacillus subtilis*), and  $\alpha$ -Synuclein ( $\alpha$ S) (the aggregation of which is a hallmark of Parkinson's disease). We observe that they each have unique intrinsic fluorescence lifetimes, which can be used to distinguish between them. We validate our novel fluorescence lifetime measurements using circular dichroism (CD, which permits the analysis of the protein secondary structure) and atomic force microscopy (AFM, which permits the characterization of individual fibrils). In the amyloid field, the discovery of different fibril strain polymorphs is associated with different toxicity to cells<sup>26</sup> and potentially different disease outcomes. Hence, to better elucidate the pathology of amyloid misfolding diseases, it is useful to efficiently identify different fibril polymorphs.<sup>27,28</sup> In the case of  $\alpha$ S, we show different distributions of fibril polymorphs are formed in “no salt” and “salt” (i.e., mimicking the physiological environment in cells) conditions, which can be distinguished using 2P-FLIM measurements. We further show an increased fluorescence

lifetime when amyloid proteins are disaggregated, indicating structural changes to the amyloids lead to changes in the fluorescence lifetime that can be tracked.

Currently, the best method to distinguish between amyloid polymorphs is cryogenic electron microscopy (cryoEM) due to its high resolution, yet it is a technique that not all researchers have access to, is expensive, and has low throughput. Another high-resolution technique is hydrogen–deuterium exchange mass spectrometry<sup>33</sup> of fibrils, which can identify differences in solvent-exposed regions, but again needs trained users and expensive equipment. More common techniques include AFM<sup>31</sup> and antibody binding or proteolysis profiles of fibrils,<sup>32</sup> all of which suffer from low throughput. We therefore provide a cheaper, more rapid, and higher-throughput technique to identify different amyloid fibrils.

## EXPERIMENTAL SECTION

**Circular Dichroism.** Protein samples were diluted to 2.5  $\mu$ M and analyzed in a 1 mm cuvette at 20 °C. CD spectra were acquired using a JASCO J-810 spectropolarimeter (Jasco Inc., Easton, MD, USA). Spectra were recorded over the spectral range of 250 – 200 nm, with a resolution of 0.5 nm, a continuous scan at 50 nm min<sup>-1</sup>, and a bandwidth resolution of 1 nm. Ten accumulations were obtained for each sample, and three preparations of each protein and buffer condition were measured. CD spectra of buffer only were recorded and subtracted from each sample spectrum. The mean residue ellipticity was calculated using eq 1

$$[\theta] = \frac{\theta_{\text{obs}}}{lcn} \quad (1)$$

where  $[\theta]$  is the mean residue ellipticity ( $^{\circ}$  cm<sup>2</sup> dmol<sup>-1</sup>),  $\theta_{\text{obs}}$  is the observed ellipticity,  $l$  is the path length (mm),  $c$  is the molar concentration, and  $n$  is the number of residues [i.e., 140 amino acids (a.a.) for  $\alpha$ S, 233 a.a. for TasA, and 162 a.a. for  $\beta$ LG].

**Fluorescence Characterization.** Protein samples were loaded into a cuvette at 100  $\mu$ M at room temperature and placed into a spectrophotometer (F-4500, Hitachi, Tokyo, Japan). Excitation and emission spectra were captured by emissions at 440 nm over a frequency sweep between 280–420 nm (at 1 nm intervals), and excitation at 370 nm over 400–500 nm (at 1 nm intervals), with emission slits of 10 nm and a scan speed of 240 nm min<sup>-1</sup>. The fluorescence spectra of the buffer were subtracted from the protein spectra. Measurements were based on triplicate measurements of three individual protein preparations. For the final plot, a MATLAB (MathWorks, Natick, MA, USA) script was used to identify the peak excitation and emission wavelengths and normalize the spectra across a range of 16 nm centered on the peak values.

**2P-FLIM.** Samples were imaged on a home-built confocal fluorescence microscope equipped with a TCSPC module. A pulsed, femtosecond Ti:S laser (MaiTai DeepSee, SpectraPhysics, Oxford, UK) provided excitation at 740 nm and a repetition rate of 80 MHz. This was passed into a commercial microscope frame (IX83, Olympus, Tokyo, Japan) through a 60 $\times$  oil objective (PlanApo 60XOSC2, 1.4 NA, Olympus). A bandpass filter of 450/50 (Chroma Technologies, Rockingham, VT, USA) was applied to the 2P emission to separate it from the excitation light. Laser scanning was performed using a galvanometric mirror system (Quadscanner, Aberrior, Göttingen, Germany). Emission photons were collected on a photon multiplier tube (PMT, PMC150, B&H GmbH, Berlin,

Germany) and relayed to a TCSPC card (SPC830, B&H GmbH). Images were acquired at  $256 \times 256$  pixels for 200 s (i.e., 20 cycles of 10 s). Photon counts were kept below 1% of SYNC rates to prevent photon pile-up. TCSPC images were analyzed using an in-house phasor plot analysis script (<https://github.com/LAG-MNG-CambridgeUniversity/TCSPCPhasor>). A general introduction to phasor plots is given in S9. 10–12 images of each sample were taken over three individual protein preparations.

**Atomic Force Microscopy.** Fibrils were directly deposited or diluted to  $10 \mu\text{M}$  in  $\text{dH}_2\text{O}$  and incubated on poly-L-lysine (Merck KGaA)-coated mica for 30 min. To remove salts, the mica was washed thrice with  $\text{dH}_2\text{O}$  and dried under a gentle stream of  $\text{N}_2$ . Imaging was performed on a BioScope Resolve (Bruker GmbH, Karlsruhe, Germany). The instrument was operated in the ScanAsyst air mode with a silicon nitride tip with a spring constant of  $40 \text{ N m}^{-1}$  and a nominal tip diameter of 2 nm (SCANASYST-AIR, Bruker). Images were collected at a scan rate of 1 Hz and a resolution of  $512 \times 512$  pixels.

**Limited Proteolysis of  $\alpha\text{S}$  Fibrils.**  $100 \mu\text{M}$  of  $\alpha\text{S}$  fibrils were incubated at  $37^\circ\text{C}$  in  $3.8 \mu\text{g mL}^{-1}$  proteinase K.  $10 \mu\text{L}$  aliquots were removed at time points of 0, 1, 5, and 15 min and incubated with 20 mM PMSF to inactivate the proteinase K. The samples were frozen and lyophilized using a LyoQuest-85 freeze dryer (Telstar, Spain). The protein films were solubilized in hexafluoro-2-propanol (HFIP). HFIP was then evaporated under a stream of  $\text{N}_2$  and the samples were resuspended in LDS buffer before being heated to  $100^\circ\text{C}$  and analyzed by SDS-PAGE on a 4–12% Bis-Tris gel (NuPAGE, Thermo Scientific) and stained with Coomassie blue (Merck KGaA).

## RESULTS

We initially performed structural and optical characterization of the three fibrillar proteins of interest (Figure 1). First, we used CD to determine the secondary structure of proteins. The method measures changes in the ellipticity of circularly polarized light when absorbed by different secondary structures (e.g.,  $\beta$ -sheet and  $\alpha$ -helix) of the protein. We observe that  $\alpha\text{S}$  (pink) has the highest proportion of  $\beta$ -sheets (i.e., the lowest mean residue ellipticity  $\sim 220 \text{ nm}$ ) compared to both  $\beta\text{LG}$  (blue) and TasA (magenta) (Figure 1a). Monomeric  $\alpha\text{S}$  is intrinsically disordered, but it undergoes structural alteration to  $\beta$ -sheets upon fibrillization.<sup>29</sup> On the other hand,  $\beta\text{LG}$  and TasA both contain  $\beta$ -sheets and  $\alpha$ -helices in their monomeric form; both proteins have a decrease in  $\alpha$ -helices and an increase in intermolecular  $\beta$ -sheets upon aggregation.<sup>30,31</sup> In order to perform physical characterization on single fibrils, we used AFM to analyze fibril morphology (Figures 1b and S2). From comparing height profiles, TasA fibrils are evidently shorter in height at  $1.0 \pm 0.3 \text{ nm}$  and without distinctive pitches in comparison to  $\beta\text{LG}$  and  $\alpha\text{S}$ , with average height profiles of  $9.5 \pm 3.6 \text{ nm}$  and  $9.0 \pm 3.2 \text{ nm}$ , respectively. For  $\beta\text{LG}$  and  $\alpha\text{S}$ , there is a relatively large spread in the height of fibrils formed, which indicates the heterogeneity that exists within the same species sample. Single-photon spectrofluorometric measurements reveal that the intrinsic fluorescence for each different amyloid has different optimal excitation and emission wavelengths in the near-UV and visible ranges, respectively, ( $\beta\text{LG}$ —ex 360 nm, em 430 nm, TasA—ex 350 nm, em 435 nm, and  $\alpha\text{S}$ —380 nm, em 425 nm, Figure 1c) and this suggests that they can be excited by 2P.

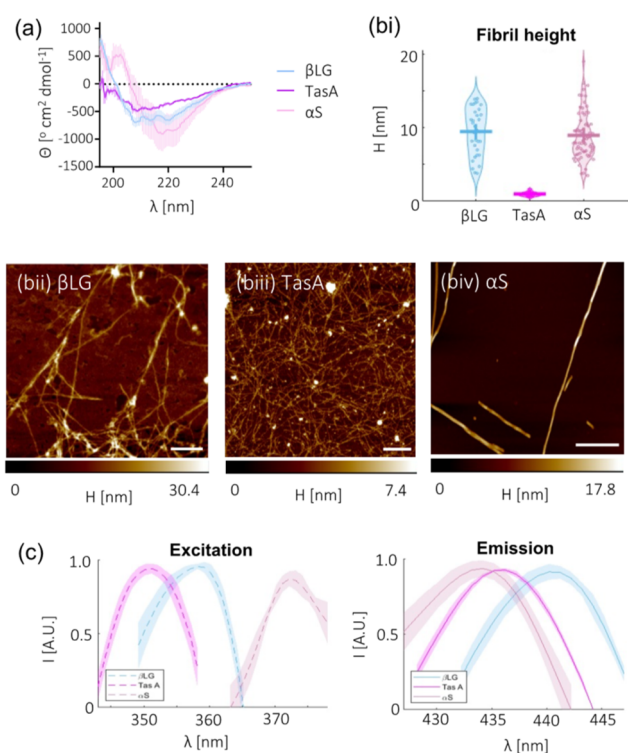


**Figure 1.** Different amyloid species can be differentiated by their spectral signatures. (a) CD spectra, displayed as the mean ellipticity per residue ( $\Theta$ ), show that  $\alpha\text{S}$  (pink) has a higher  $\beta$ -sheet content than  $\beta\text{LG}$  (blue) and TasA (magenta). (b) Representative AFM images show the resulting amyloid fibrils have different morphologies. A height quantification is given in (bi). (bii)  $\beta\text{LG}$  fibrils are on average  $9.5 \pm 3.6 \text{ nm}$  in height (quoted as mean  $\pm$  SD). (biii) TasA fibrils have no periodicity and are on average  $1.0 \pm 0.3 \text{ nm}$  in height. (biv)  $\alpha\text{S}$  fibrils have mixed polymorphs with only some fibrils displaying periodicity and an average height of  $9.0 \pm 3.2 \text{ nm}$ . (c) Excitation and emission peaks for each protein are,  $\beta\text{LG}$ —ex 360 nm, em 430 nm, TasA—ex 350 nm, em 435 nm, and  $\alpha\text{S}$ —380 nm, em 425 nm.

We next investigated the intrinsic fluorescence lifetime signatures of the three amyloid fibril samples using 2P-FLIM. We also image the sample topography using AFM, as the diffraction limit on our 2P-FLIM system does not permit the visualization of small fibrils. We deposit fibrils washed in  $\text{dH}_2\text{O}$  at  $100 \mu\text{M}$  onto clean glass coverslips, which are then dried before imaging to provide a dense coverage of the protein (Figure 2a, AFM). The lifetime of the intrinsic fluorescence emission reveals that all the amyloids possess complex exponentials with phasors that fall within the universal semicircle (i.e., which denotes monoexponential lifetimes) of the phasor plot (Figure 2b) and in distinct positions from one another. Moreover, there are significant differences in their modulation ( $\tau_M$ ) and phase ( $\tau_\phi$ ) lifetimes; for comparison of the fluorescence lifetime,  $\tau_M$  will be quoted henceforth as it is more sensitive than  $\tau_\phi$ . We measure that  $\beta\text{LG}$  has the highest fluorescence lifetime at  $1.7 \pm 0.2 \text{ ns}$ , in comparison to TasA ( $0.96 \pm 0.02 \text{ ns}$ ) and  $\alpha\text{S}$  ( $1.1 \pm 0.1 \text{ ns}$ ) (Figure 2c). We note that monomeric fluorescence is too weak to be detected on our 2P-FLIM system; indeed, spectrophotometric measurements show a 100-fold difference in fluorescence intensity between the fibrillar and monomeric forms of  $\alpha\text{S}$  (Figure S3).

It has been suggested that structurally different  $\alpha\text{S}$  fibril polymorphs can lead to different synucleopathies due to

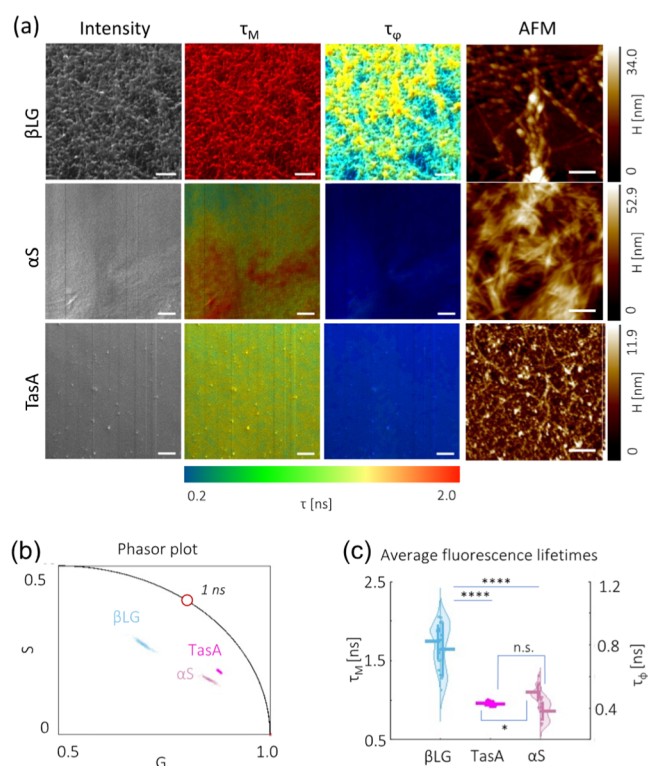


**Figure 2.**  $\beta$ LG, TasA, and  $\alpha$ S display different intrinsic fluorescent lifetime signatures. (a) Fluorescence intensity, fluorescence lifetime (i.e., both  $\tau_M$  and  $\tau_\phi$ ), and AFM representative images are shown. Their fluorescence lifetimes follow a multiexponential decay, as seen from the differences in calculated  $\tau_M$  and  $\tau_\phi$  (denoting that these phasors lie within the universal semicircle). Scale bars, 10  $\mu$ m (FLIM) and 400 nm (AFM). (b,c) Phasor plots and average calculated fluorescence lifetimes show that each amyloid has a distinctive lifetime, but that of  $\beta$ LG is significantly higher.

differences in membrane binding, seeding behavior, and toxicity.<sup>32–34</sup> Results in Figure 2 clearly show that different amyloids can be distinguished by their fluorescence lifetime signatures. Hence, this encouraged us to investigate if fluorescence lifetime is also responsive to more subtle structural changes, for example, polymorphic variants that emerge for the same protein when aggregated under different buffer conditions. It has previously been shown that “no salt” and “salt” aggregation buffer conditions induce the formation of mixed populations of  $\alpha$ S polymorphs, where fibrils formed in high salt conditions have distinct periodic pitches instead of flat ribbon structures.<sup>35</sup> Our “no salt” condition contains 10 mM Tris pH 7.4 (denoted as Tris) and two “salt” conditions feature the addition of 2 mM  $\text{CaCl}_2$  and 140 mM NaCl ( $\text{CaCl}_2/\text{NaCl}$ , i.e., extracellular mimicking) and 140 mM KCl (KCl, i.e., intracellular mimicking). 2P-FLIM measurements show lowered fluorescence lifetimes for  $\alpha$ S fibrils formed in KCl ( $0.95 \pm 0.09$  ns) or  $\text{CaCl}_2/\text{NaCl}$  salts ( $0.96 \pm 0.05$  ns) compared to  $\alpha$ S when aggregated in just Tris buffer ( $1.1 \pm 0.1$  ns) (Figure 3). Although the magnitude of the difference is slight compared to those between different amyloid species (Figure 2), this is as expected as there are fewer structural and molecular packing differences between the  $\alpha$ S samples than between different protein species. Moreover, their fluorescence spectra (Figure S4) also show similar optimal excitation and emission wavelengths.

We then further characterized the three  $\alpha$ S fibril samples to determine whether they are truly structurally and/or morphologically different. Two-dimensional (2D) and three-dimensional (3D) AFM images show several different  $\alpha$ S fibril polymorphs within each buffer condition (Figures 3d,e and S5). These polymorphs can be classified as either smooth (pink arrows), periodic (green arrows), or twisted periodic, likely arising from two fibrils twisting around each other (blue arrows). We performed single-fibril analysis based on AFM images to classify the height distribution and the prevalence of periodicity within each sample. As before, we observe a wide range of heights of fibrils within the same sample, with an average height of  $9.0 \pm 3.2$  nm (Tris),  $9.6 \pm 2.9$  nm ( $\text{CaCl}_2/\text{NaCl}$ ), and  $10.2 \pm 3.3$  nm (KCl) (Figure 3f). The addition of salts promotes the formation of higher and intertwined fibrils, of which a greater proportion of those being periodic (i.e., 72 and 76% for  $\text{CaCl}_2/\text{NaCl}$  and KCl, respectively, in comparison to 70% for Tris, Figure 3fv). This is most apparent in the  $\alpha$ S fibrils formed in KCl, where the fibril height distribution is more bimodal, showing single-fibril height and double-fibril height (Figure 3fi). In general, fibrils aggregated in salt buffers are higher with a lower frequency of pitches. The addition of salts slightly increases the chance of periodic fibrils over flat ones. CD measurements show that  $\alpha$ S aggregated in salt buffers has a decreased  $\beta$ -sheet content compared to those in Tris (Figure 3g). Furthermore, differences in fibril proteolysis profiles can be used to indicate a different fibril structure and core due to differences in the accessibility of the protease.<sup>32</sup> 100  $\mu$ M of  $\alpha$ S in each buffer condition were incubated in proteinase K for 0, 1, 5, and 15 min. Monomeric  $\alpha$ S has a molecular weight of  $\sim 14.4$  kDa. Limited proteolysis of the  $\alpha$ S fibrils in the three buffers with proteinase K shows similar digestion profiles, but differing band intensities, indicating similarities in the core structure, but differences in the fibril packing and accessibility of proteinase K to the cleavage sites in the different fibril samples (Figure 3h, with a repeat shown in Figure S6). Therefore, our sample characterization supports structural differences in the fibrils formed under different salt conditions, which we observe to possess different fluorescence lifetimes.

Lastly, to validate the use of intrinsic fluorescence lifetime as an in vitro label-free aggregation assay, we disaggregated fibrillar  $\alpha$ S and  $\beta$ LG by mixing the samples with HFIP, a solvent typically used to monomerize proteins before aggregation. We observe the formation of shortened fibrils and oligomers in  $\alpha$ S and  $\beta$ LG, respectively, in AFM images (Figure 4a, AFM). Correspondingly, these disaggregated structures lead to significantly increased fluorescence lifetimes, especially in the case of oligomeric  $\beta$ LG ( $2.6 \pm 0.1$  ns from  $1.7 \pm 0.2$  ns) and less so for  $\alpha$ S ( $1.2 \pm 0.06$  ns from  $1.1 \pm 0.1$  ns) (Figure 4b,c). As the intrinsic amyloid fluorescence could still be detected from both samples, this insinuates that there is still  $\beta$ -sheet stacking present in the disaggregated structures of  $\beta$ LG and  $\alpha$ S, yet a change in the stacking or arrangement during partial disaggregation has led to a change in the intrinsic fluorescence lifetime.

## DISCUSSION

There is a need for label-free techniques to identify and monitor aggregation of amyloid proteins that is currently unmet. Here, we use a combination of structural and morphological techniques to validate the use of 2P-FLIM in identifying different amyloid protein fibrils, their polymorphs,

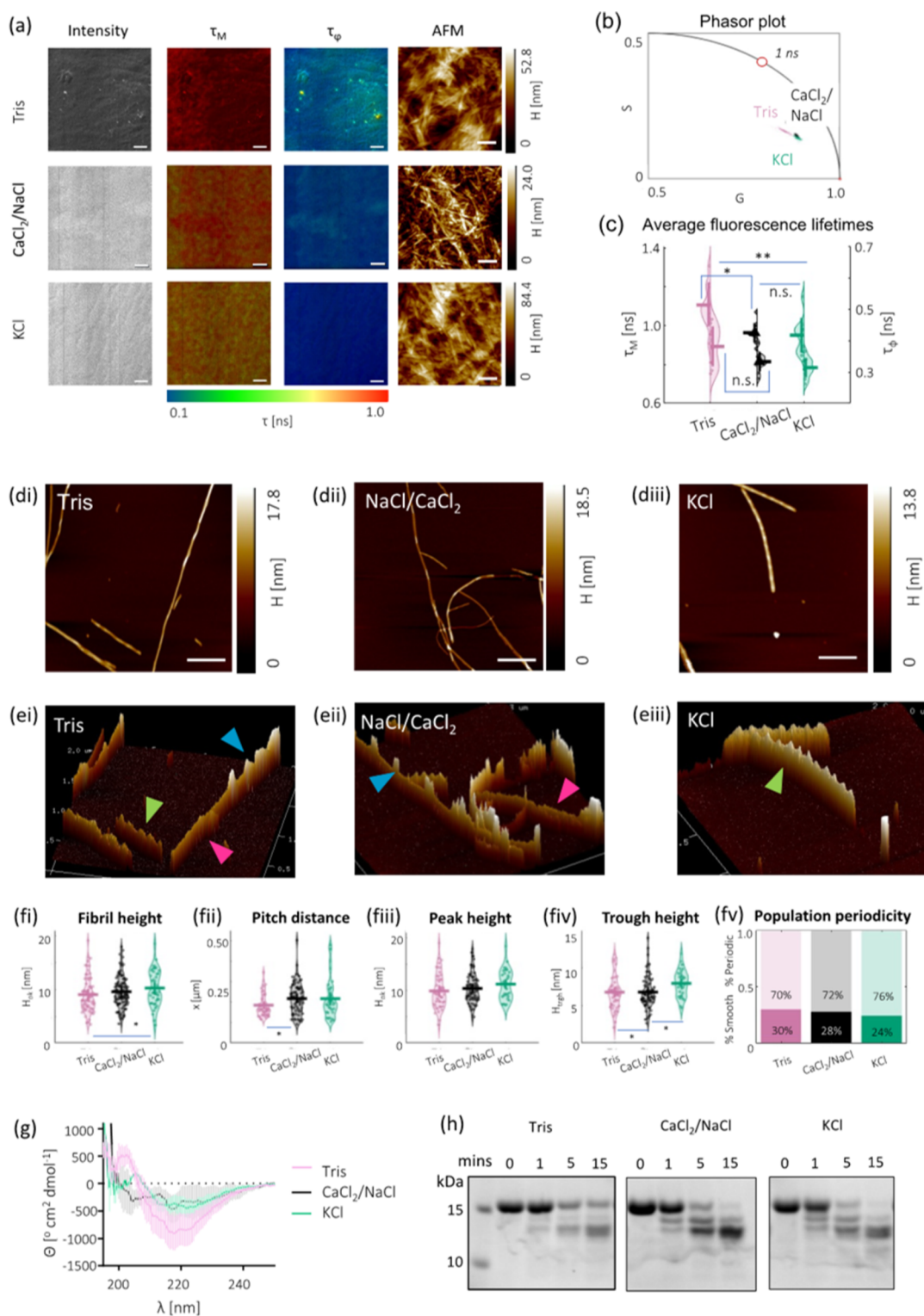


**Figure 3.**  $\alpha S$  aggregated in salt buffers exhibits lower fluorescence lifetimes due to variation in the distribution of their polymorphs. (a) Fluorescence intensity,  $\tau_M$  and  $\tau_{\phi}$ , and AFM representatives are shown for  $\alpha S$  fibrils formed in Tris,  $\text{CaCl}_2/\text{NaCl}$ , and KCl. Scale bars, 10  $\mu\text{m}$  (FLIM) and 400 nm (AFM). (b,c) Phasor plots show that  $\alpha S$  fibrils formed in salts have a lower average fluorescence lifetime compared to those formed in Tris only. Shown are (d) 2D and (e) 3D AFM images of individual fibrils in different buffers. Different morphologies are indicated by colored arrows, that is, flat (pink), twisted periodic, from intertwined fibrils (blue), and periodic (green). (f) Quantification of fibrils shows that there is great heterogeneity within each sample. (g) CD of 2.5  $\mu\text{M}$  of each protein fibril shows that  $\alpha S$  in Tris has a higher  $\beta$ -sheet content compared to  $\alpha S$  in KCl and  $\text{CaCl}_2/\text{NaCl}$ . (h) Degradation patterns of the three samples show a similar band profile, but the intensities differ, indicating differences in cleavage rates.

and their disaggregated states using fluorescence lifetime imaging. We investigate three amyloid proteins:  $\beta\text{LG}$ , TasA,

and  $\alpha S$ . For conventional fluorophores, for example, GFP, their fluorescence lifetime is influenced by the surrounding environ-

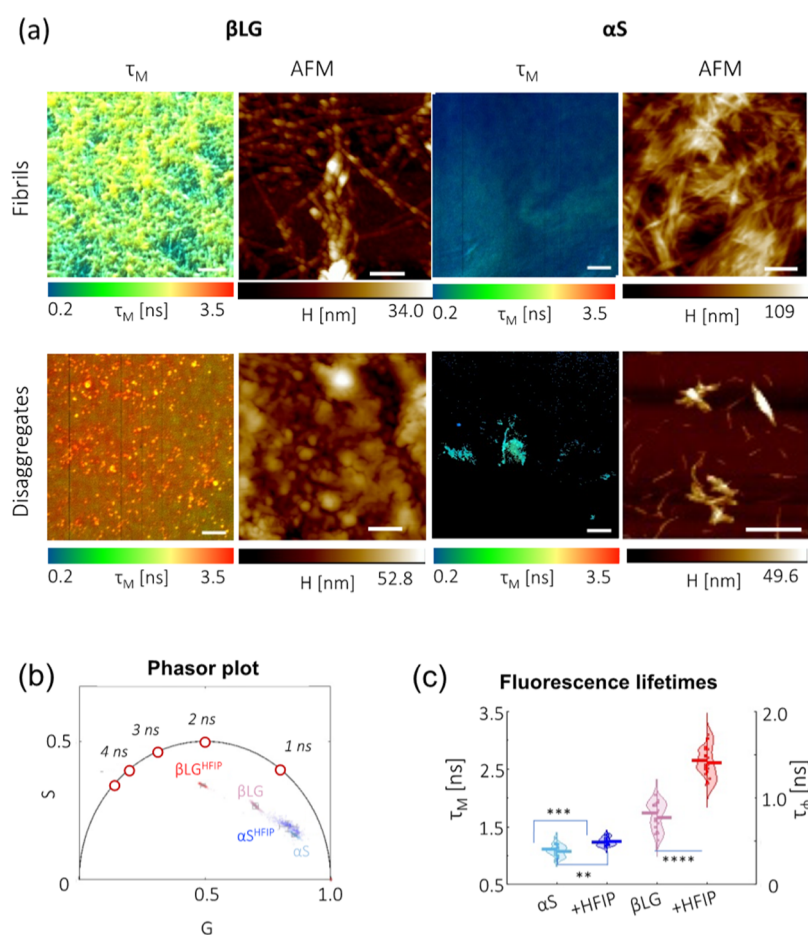


**Figure 4.** Fluorescence lifetime change of different amyloid proteins upon aggregation is reversible, with disaggregated structures of  $\alpha$ S and  $\beta$ LG having higher fluorescence lifetimes than their fibrillar counterparts. (a) Fluorescence lifetimes and AFM images comparing  $\alpha$ S and  $\beta$ LG fibrils before and after disaggregation by HFIP. Scale bars, 10  $\mu$ m (FLIM) and 400 nm (AFM). (b,c) Phasor plots and average fluorescence lifetimes show a significant decrease in the fluorescence lifetime after the addition of HFIP to disaggregate the fibrils for both  $\alpha$ S and  $\beta$ LG.

ment.<sup>36</sup> The field of intrinsic nonaromatic fluorescence is comparatively young, therefore studies into differences in amyloid structures and their interaction with the local environment have not yet been fully conducted. The intrinsic fluorescence lifetime of amyloid fibrils may well be influenced by fibril packing and environmental interactions, which can lead to unique lifetimes for different proteins and polymorphs. Here, we present the unique intrinsic fluorescence lifetime signatures of different amyloids, using model-free phasor plot analysis.

We then investigated whether 2P-FLIM could be used to identify fibril polymorphs of the same protein. The fibril formation of  $\alpha$ S is implicated in several neuropathological diseases, including but not limited to, Parkinson's disease, dementia with Lewy bodies, and multiple system atrophy (MSA).<sup>37</sup> Although cryoEM is a gold standard for the identification of fibril polymorphs, it is an expensive technique that requires skilled users and has low throughput. Here, we use 2P-FLIM and show that  $\alpha$ S fibrils formed in salt buffers mimicking the intracellular and extracellular environments have a slightly quenched fluorescence lifetime compared to the polymorphs formed without salt. From a structural perspective, noting that the fibrils are washed in H<sub>2</sub>O prior to 2P-FLIM imaging to remove salt ions, this quenching effect could be attributed to differences in the fibril packing (from limited proteolysis) or  $\beta$ -sheet structure (from CD), leading to the

formation of different fibril polymorphs, that appear to have higher fibrils and less frequent pitches (from AFM). We identify bigger differences between the “no salt” Tris buffer sample and the salt samples, showing that the fibrils formed in Tris buffer are different to those formed in salt and thus are unlikely to be physiologically relevant. There is a slight but insignificant difference in the fluorescence lifetimes, which is lower for  $\alpha$ S fibrils formed in KCl than in CaCl<sub>2</sub>/NaCl. A recent study has shown that  $\alpha$ S isolated from the brains of MSA patients differs from those formed from recombinant  $\alpha$ S aggregated in vitro.<sup>38</sup> In the future, it would be interesting to assess structures isolated from tissues to determine whether in vivo amyloids can be distinguished using 2P-FLIM, as we have shown for the three in vitro assembled protein amyloid fibrils, and whether polymorphic  $\alpha$ S structures isolated from different cell types can also be uniquely identified. Furthermore, structural analysis using mutants and computational simulations may be able to pin-point the mechanisms that derive differences in the fluorescence lifetime.

To quantify structural differences, we show that disaggregating preformed fibrils of  $\alpha$ S and  $\beta$ LG results in an increase in their fluorescence lifetimes. We believe this stems from the looser packing and reduction  $\beta$ -sheets within the disaggregated structures (i.e., smaller fibrils for  $\alpha$ S and oligomers for  $\beta$ LG).<sup>39</sup>

## CONCLUSIONS

We validate that the intrinsic amyloid fluorescence lifetime can be used as a label-free method to characterize different amyloid proteins, and the distribution within polymorphic populations of  $\alpha$ S and disaggregated structures. Our current work comprises observations on intrinsic amyloid fluorescence, which we find is affected by several different factors, for example, the  $\beta$ -sheet content and molecular packing. 2P-FLIM and efficient phasor plot analysis of fluorescence lifetimes may be useful if applied to drug screening for amyloid protein-targeting compounds, as 2P-FLIM can circumvent issues with small-molecule interference with fluorescence intensity-based assays. To complement our findings, we believe that computational studies on the molecular structure of these amyloids at an atomistic scale that permit the study of electron transitions would be needed to establish causative links between the structure and the unique fluorescence lifetime signatures that amyloids possess. The intrinsic amyloid fluorescence lifetime in conjunction with fit-free phasor plot analysis provides a medium throughput, efficient, and label-free method to distinguish between different amyloids and their polymorphs.

## ASSOCIATED CONTENT

### Supporting Information

The Supporting Information is available free of charge at <https://pubs.acs.org/doi/10.1021/acs.analchem.1c05651>.

Experimental methods and supplementary figures (PDF)  
All raw data is available at the Cambridge University Repository (DOI: 10.17863/CAM.82267).

## AUTHOR INFORMATION

### Corresponding Author

Gabriele S. Kaminski Schierle – Department of Chemical Engineering and Biotechnology, Phillipa Fawcett Drive, University of Cambridge, Cambridge CB3 0AS, U.K.; [orcid.org/0000-0002-1843-2202](https://orcid.org/0000-0002-1843-2202); Email: [gsk20@cam.ac.uk](mailto:gsk20@cam.ac.uk)

### Authors

Chyi Wei Chung – Department of Chemical Engineering and Biotechnology, Phillipa Fawcett Drive, University of Cambridge, Cambridge CB3 0AS, U.K.; [orcid.org/0000-0003-1780-3486](https://orcid.org/0000-0003-1780-3486)

Amberley D. Stephens – Department of Chemical Engineering and Biotechnology, Phillipa Fawcett Drive, University of Cambridge, Cambridge CB3 0AS, U.K.; [orcid.org/0000-0002-7303-6392](https://orcid.org/0000-0002-7303-6392)

Edward Ward – Department of Chemical Engineering and Biotechnology, Phillipa Fawcett Drive, University of Cambridge, Cambridge CB3 0AS, U.K.

Yuqing Feng – Department of Chemical Engineering and Biotechnology, Phillipa Fawcett Drive, University of Cambridge, Cambridge CB3 0AS, U.K.

Molly Jo Davis – Department of Chemical Engineering and Biotechnology, Phillipa Fawcett Drive, University of Cambridge, Cambridge CB3 0AS, U.K.

Clemens F. Kaminski – Department of Chemical Engineering and Biotechnology, Phillipa Fawcett Drive, University of Cambridge, Cambridge CB3 0AS, U.K.; [orcid.org/0000-0002-5194-0962](https://orcid.org/0000-0002-5194-0962)

Complete contact information is available at:  
<https://pubs.acs.org/10.1021/acs.analchem.1c05651>

## Author Contributions

C.W.C. and A.D.S. contributed equally. G.S.K.S., C.W.C., and A.D.S. conceived the manuscript. C.W.C., A.D.S., Y.F., and M.J.D. prepared the protein for experiments. C.W.C. and E.W. built the 2P-FLIM, C.W.C. collected the 2P-FLIM data, and C.W.C. analyzed the 2P-FLIM data. C.W.C. collected the excitation and emission spectra. A.D.S. collected the CD data. C.W.C. and A.D.S. collected the AFM data and C.W.C. analyzed the AFM data. A.D.S. performed limited proteolysis. C.F.K. provided the equipment. All the authors contributed to paper writing. All the authors have given approval to the final version of the paper.

## Notes

The authors declare no competing financial interest.

## ACKNOWLEDGMENTS

C.W.C. is jointly funded by the Cambridge Trust and Wolfson College for her PhD. G.S.K.S. acknowledges funding from the Wellcome Trust (065807/Z/01/Z) (203249/Z/16/Z), the UK Medical Research Council (MR/K02292X/1), Alzheimer's Research UK (ARUK) (ARUK-PG013-14), the Michael J. Fox Foundation (16238), and Infinitus China Ltd. M.J.D. was funded by the NanoDTC EPSRC Grant EP/S022953/1. We thank Naunehal Matharu for preliminary CD data not in the final manuscript and Maria Zacharopoulou for discussions on  $\alpha$ S fibril polymorphs.

## REFERENCES

- (1) Guerrero-Ferreira, R.; Kovacic, L.; Ni, D.; Stahlberg, H. *Curr. Opin. Neurobiol.* **2020**, *61*, 89–95.
- (2) Biancalana, M.; Koide, S. *Biochim. Biophys. Acta, Proteins Proteomics* **2010**, *1804*, 1405–1412.
- (3) Mikalauskaite, K.; Ziaunys, M.; Sneideris, T.; Smirnovas, V. *Int. J. Mol. Sci.* **2020**, *21*, 8916.
- (4) Hackl, E. V.; Darkwah, J.; Smith, G.; Ermolina, I. *Eur. Biophys. J.* **2015**, *44*, 249–261.
- (5) Pinotsi, D.; Buell, A. K.; Dobson, C. M.; Kaminski Schierle, G. S.; Kaminski, C. F. *ChemBioChem* **2013**, *14*, 846–850.
- (6) Sidhu, A.; Vaneyck, J.; Blum, C.; Segers-Nolten, I.; Subramaniam, V. *Amyloid* **2018**, *25*, 189–196.
- (7) Anderson, V. L.; Webb, W. W. *BMC Biotechnol.* **2011**, *11*, 1–10.
- (8) Afitska, K.; Fucikova, A.; Shvadchak, V. v.; Yushchenko, D. A. *Biophys. J.* **2017**, *113*, 2182–2191.
- (9) Cosentino, M.; Canale, C.; Bianchini, P.; Diaspro, A. *Sci. Adv.* **2019**, *5*, No. eaav8062.
- (10) Pinotsi, D.; Grisanti, L.; Mahou, P.; Gebauer, R.; Kaminski, C. F.; Hassanali, A.; Kaminski Schierle, G. S. *J. Am. Chem. Soc.* **2016**, *138*, 3046–3057.
- (11) Stephens, A. D.; Qaisrani, M. N.; Ruggiero, M. T.; Diaz Mirón, G.; Morzan, U. N.; González Lebrero, M. C.; Jones, S. T. E.; Poli, E.; Bond, A. D.; Woodhams, P. J.; Kleist, E. M.; Grisanti, L.; Gebauer, R.; Zeitler, J. A.; Credgington, D.; Hassanali, A.; Kaminski Schierle, G. S. *Proc. Natl. Acad. Sci. U.S.A.* **2021**, *118* (21), e2020389118.
- (12) Chan, F. T. S.; Kaminski Schierle, G. S.; Kumita, J. R.; Bertoncini, C. W.; Dobson, C. M.; Kaminski, C. F. *Analyst* **2013**, *138*, 2156–2162.
- (13) Shukla, A.; Mukherjee, S.; Sharma, S.; Agrawal, V.; Radha Kishan, K. V.; Guptasarma, P. *Arch. Biochem. Biophys.* **2004**, *428*, 144–153.
- (14) del Mercato, L. L.; Pompa, P. P.; Maruccio, G.; Torre, A. D.; Sabella, S.; Tamburro, A. M.; Cingolani, R.; Rinaldi, R. *Proc. Natl. Acad. Sci. U.S.A.* **2007**, *104*, 18019–18024.
- (15) Becker, W. J. *Microsc.* **2012**, *247*, 119–136.
- (16) Hecker, L.; Wang, W.; Mela, I.; Fathi, S.; Poudel, C.; Soavi, G.; Huang, Y. Y. S.; Kaminski, C. F. *Nano Lett.* **2021**, *21*, 938–945.

- (17) Denk, W.; Strickler, J. H.; Webb, W. W. *Science* **1990**, *248*, 73–76.
- (18) Benninger, R. K. P.; Piston, D. W. *Curr. Protoc. Cell Biol.* **2013**, *59*, 4–11.
- (19) Larson, A. M. *Nat. Photonics* **2010**, *5*, 1.
- (20) Moulton, P. F. *J. Opt. Soc. Am. B* **1986**, *3*, 125–133.
- (21) Svoboda, K.; Yasuda, R. *Neuron* **2006**, *50*, 823–839.
- (22) Miller, D. R.; Jarrett, J. W.; Hassan, A. M.; Dunn, A. K. *Curr. Opin. Biomed. Eng.* **2017**, *4*, 32–39.
- (23) Ranjit, S.; Malacrida, L.; Jameson, D. M.; Gratton, E. *Nat. Protoc.* **2018**, *13*, 1979–2004.
- (24) Liao, S.-C.; Sun, Y.; Coskun, U. *FLIM analysis using the phasor plots*; ISS, 2014.
- (25) Digman, M. A.; Caiolfa, V. R.; Zama, M.; Gratton, E. *Biophys. J.* **2008**, *94*, L14.
- (26) Peng, C.; Gathagan, R. J.; Lee, V. M.-Y. *Neurobiol. Dis.* **2018**, *109*, 209–218.
- (27) Li, B.; Ge, P.; Murray, K. A.; Sheth, P.; Zhang, M.; Nair, G.; Sawaya, M. R.; Shin, W. S.; Boyer, D. R.; Ye, S.; Eisenberg, D. S.; Zhou, Z. H.; Jiang, L. *Nat. Commun.* **2018**, *9*, 3609.
- (28) Guerrero-Ferreira, R.; Kovacic, L.; Ni, D.; Stahlberg, H. *Curr. Opin. Neurobiol.* **2020**, *61*, 89–95.
- (29) Ruggeri, F. S.; Benedetti, F.; Knowles, T. P. J.; Lashuel, H. A.; Sekatskii, S.; Dietler, G. *Proc. Natl. Acad. Sci. U.S.A.* **2018**, *115*, 7230–7235.
- (30) Landureau, M.; Redeker, V.; Bellande, T.; Eyquem, S.; Melki, R. *J. Biol. Chem.* **2021**, *296*, 100737.
- (31) Giasson, B. I.; Murray, I. V. J.; Trojanowski, J. Q.; Lee, V. M.-Y. *J. Biol. Chem.* **2001**, *276*, 2380–2386.
- (32) Ioannou, J. C.; Donald, A. M.; Tromp, R. H. *Food Hydrocolloids* **2015**, *46*, 216–225.
- (33) Chai, L.; Romero, D.; Kayatekin, C.; Akabayov, B.; Vlamakis, H.; Losick, R.; Kolter, R. *J. Biol. Chem.* **2013**, *288*, 17559.
- (34) Meade, R. M.; Williams, R. J.; Mason, J. M. *NPJ Parkinson's dis.* **2020**, *6*, 17.
- (35) de Giorgi, F.; Laferrière, F.; Zinghirino, F.; Faggiani, E.; Lends, A.; Bertoni, M.; Yu, X.; Grélard, A.; Morvan, E.; Habenstein, B.; Dutheil, N.; Doudnikoff, E.; Daniel, J.; Claverol, S.; Qin, C.; Loquet, A.; Bezard, E.; Ichas, F. *Sci. Adv.* **2020**, *6*, No. eabc4364.
- (36) Gath, J.; Bousset, L.; Habenstein, B.; Melki, R.; Böckmann, A.; Meier, B. H. *PLoS One* **2014**, *9*, No. e90659.
- (37) Berezin, M. Y.; Achilefu, S. *Chem. Rev.* **2010**, *110*, 2641–2684.
- (38) Schweighauser, M.; Shi, Y.; Tarutani, A.; Kametani, F.; Murzin, A. G.; Ghetti, B.; Matsubara, T.; Tomita, T.; Ando, T.; Hasegawa, K.; Murayama, S.; Yoshida, M.; Hasegawa, M.; Scheres, S. H. W.; Goedert, M. *Nature* **2020**, *585*, 464–469.
- (39) Chen, S. W.; Drakulic, S.; Deas, E.; Ouberaï, M.; Aprile, F. A.; Arranz, R.; Ness, S.; Roodveldt, C.; Guilliams, T.; De-Genst, E. J.; Klenerman, D.; Wood, N. W.; Knowles, T. P. J.; Alfonso, C.; Rivas, G.; Abramov, A. Y.; Valpuesta, J. M.; Dobson, C. M.; Cremades, N. *Proc. Natl. Acad. Sci. U.S.A.* **2015**, *112*, E1994–E2003.